Colloids and Surfaces B: Biointerfaces 102 (2013) 441–449

Contents lists available at SciVerse ScienceDirect

Colloids and Surfaces B: Biointerfaces

journal homepage: www.elsevier.com/locate/colsurfb

# Poly(ε-caprolactone), Eudragit® RS 100 and poly(ε-caprolactone)/Eudragit® RS 100 blend submicron particles for the sustained release of the antiretroviral efavirenz

Katia P. Seremeta[a,b], Diego A. Chiappetta[a,b], Alejandro Sosnik[a,b,*]

[a] The Group of Biomaterials and Nanotechnology for Improved Medicines (BIONIMED), Department of Pharmaceutical Technology, Faculty of Pharmacy and Biochemistry, University of Buenos Aires, 956 Junín St., Buenos Aires CP1113, Argentina
[b] National Science Research Council (CONICET), Buenos Aires, Argentina

ARTICLE INFO

*Article history:*
Received 7 May 2012
Received in revised form 12 June 2012
Accepted 24 June 2012
Available online xxx

*Keywords:*
HIV infection
Antiretrovirals
Efavirenz-loaded poly(ε-caprolactone), Eudragit® RS 100 and poly(ε-caprolactone)/Eudragit® RS 100 blend submicron particles
Drug delivery systems
Controlled release *in vitro*

ABSTRACT

The design of simple and scalable drug delivery systems to target the central nervous system (CNS) could represent a breakthrough in the addressment of the HIV-associated neuropathogenesis. The intranasal (i.n.) route represents a minimally invasive strategy to surpass the blood–brain barrier, though it demands the use of appropriate nanocarriers bearing high drug payloads and displaying sufficiently long residence time. The present work explored the development of submicron particles made of poly(ε-caprolactone) (PCL), Eudragit® RS 100 (RS a copolymer of ethylacrylate, methylmethacrylate and methacrylic acid esterified with quaternary ammonium groups) and their blends, loaded with the first-choice antiretroviral efavirenz (EFV) as an approach to fine tune the particle size and the release kinetics. Particles displaying hydrodynamic diameters between 90 and 530 nm were obtained by two methods: nanoprecipitation and emulsion/solvent diffusion/evaporation. In general, the former resulted in smaller particles and narrower size distributions. The encapsulation efficiency was greater than 94%, the drug weight content approximately 10% and the yield in the 72.5–90.0% range. The highly positive surface (>+30 mV) rendered the suspensions physically stable for more than one month. *In vitro* release assays indicated that the incorporation of the poly(methacrylate) into the composition reduced the burst effect and slowed the release rate down with respect to pure poly(ε-caprolactone) particles. The analysis of the release profile indicated that, in all cases, the kinetics adjusted well to the Higuchi model with $R^2_{adj}$ values >0.9779. These findings suggested that the release was mainly controlled by diffusion. In addition, when data were analyzed by the Korsmeyer–Peppas model, *n* values were in the 0.520–0.587 range, indicating that the drug release was accomplished by the combination of two phenomena: diffusion and polymer chain relaxation. Based on ATR/FT-IR analysis that investigated drug/polymer matrix interactions, the potential role of the hydrophobic interactions of C—F groups of EFV with carbonyl groups in the backbone of PCL and poly(methacrylate) could be ruled out. The developed EFV-loaded particles appear as a useful platform to investigate the intranasal administration to increase the bioavailability in the CNS.



## 1. Introduction

The Human Immunodeficiency Virus (HIV)/Acquired Immunodeficiency Syndrome (AIDS) is the most deadly infectious disease of our times with approximately 35 million infected people worldwide [1]. The High Activity Antiretroviral Therapy (HAART) has improved the therapeutic outcomes [2,3] and the disease has become chronic in most of the developed countries [4]. To ensure therapeutic success, patients need to adhere strictly to the administration schedule [5]. On the other hand, HAART does not eradicate the virus from the host due to the generation of intracellular and anatomical reservoirs, where the virus remains in latency and less accessible to antiretrovirals (ARVs) [6–8].

Blood–tissue barriers protect specific body compartments by constraining the passage of drugs owing to the activity of a variety of efflux pumps belonging to the ATP-binding cassette superfamily (ABC) [9,10], this phenomenon often resulting in reduced bioavailability [11]. ARVs are substrates of, at least, one pump [12–14]. ABCs are profusely distributed in the blood–brain barrier (BBB) [15] and they play a key role in the generation of the HIV reservoir in the central nervous system (CNS) [16,17]. In CNS, the virus leads to a gradual deterioration of the cognitive functions, a disease known as

* Corresponding author at: Department of Pharmaceutical Technology, Faculty of Pharmacy and Biochemistry, University of Buenos Aires, 956 Junín St., 6th Floor, Buenos Aires CP1113, Argentina. Fax: +54 11 4964 8273.
*E-mail address:* alesosnik@gmail.com (A. Sosnik).

0927-7765/$ – see front matter © 2012 Elsevier B.V. All rights reserved.
http://dx.doi.org/10.1016/j.colsurfb.2012.06.038

HIV-associated neurocognitive disorder (HAND) [18–20] that hits especially younger patients [21]. The design of simple and effective drug delivery systems that effectively target the CNS could represent a breakthrough to tackle the HIV neuropathogenesis [18,22].

Different nanocarriers are being explored to passively or actively target ARVs to the CNS [23,24]. Some works employed nanoparticles surface-decorated with ligands that are recognizable by specific receptors in the apical surface of the BBB [25]. Other research groups co-administered ARVs with different poly(ethylene oxide)–poly(propylene oxide) (PEO–PPO) amphiphiles [26] that inhibit the functional activity of ABCs and improve the bioavailability of the drug in the CNS [27,28]. Gendelman and coworkers designed an interesting cell delivery platform employing drug-loaded "macrophage ghosts" [29]. These approaches usually comprised the intravenous (i.v.) administration of the drug-loaded system.

The intranasal (i.n.) route capitalizes on the direct nose-to-brain transport that would involve the terminals of olfactory neurons present in the nasal mucosa [29–31]. The most appealing features of this administration route in HIV would be (i) minimal invasiveness, (ii) painlessness and (iii) possible self-administration [32]. Interestingly, the transport has been shown to be more effective for drugs encapsulated within submicron carriers than for drugs in solution, suggesting the involvement of active cell uptake pathways. A main limitation that precluded the translation of the i.n. route into clinics is the small volume that can be instilled in the nostril [33]. In this context, only systems containing great drug payloads would enable the attainment of sufficiently high doses.

Only a few works assessed the i.n. administration of ARV-loaded particles to target the CNS [34]. Recently, we compared the pharmacokinetics in plasma and CNS of efavirenz (EFV) encapsulated within single and mixed poloxamer and poloxamine polymeric micelles after i.n. and i.v. administration [35]. The bioavailability in the brain and the relative exposure index were increased four and five times, respectively, with respect to the systems administered i.v.; the relative index was calculated by taking the ratio between the area-under-the-curve in CNS and plasma. However, polymeric micelles could not sustain the release in the long-term range [35]. To achieve more prolonged release profiles that would ensure constant drug concentrations, a different nanocarrier has to be engineered.

Poly($\varepsilon$-caprolactone) (PCL) is a highly hydrophobic and semi-crystalline polyester that owing to its proven biocompatibility, biodegradability and permeability has found broad application in the development of drug delivery systems [36–39]. PCL has already obtained approval by the USA-Food and Drug Administration and the European Medicines Agency [40]. PCL undergoes hydrolysis and subsequent conversion into 6-hydroxylcaproic acid and acetyl-CoA *in vivo*, finally entering the citric acid pathway. *In vitro* assays in water showed that PCL degrades very slowly, though the degradation kinetics depends on its molecular weight and the size and the surface area of the implants [41,42]. Moreover, specific enzymes such as lipase catalyzed the *in vitro* degradation in approximately 1000-times [43]. The *in vivo* degradation was even faster [44].

Eudragit® comprises a series of biocompatible copolymers often used for film coating of solid formulations and the different derivatives have been accepted the regulatory agencies of USA, Europe and Japan for oral and topical administration [45]. Even though these copolymers are not biodegradable, several research groups employed Eudragit®-made nanoparticles for the parenteral administration of drugs and they reported on the good biocompatibility of this biomaterial also by these routes [46–48], owing to the rapid clearance from the systemic circulation by the mononuclear phagocytic system and their deposition in the liver [49]. Moreover, they have been used to develop tissue engineering scaffolds [50].

As a preamble to a comprehensive study of the key parameters that govern the absorption process from the olfactory mucosa (*e.g.*, particle size and composition), in the present work, we developed submicron particles made of PCL of two different molecular weights, a water-insoluble/water-permeable poly(methacrylate) (Eudragit® RS 100) and their blends loaded with the first-line ARV efavirenz (EFV). This polymer composition enabled the fine tuning of the particle size and the release profile (especially the burst effect) with respect to a control of pure PCL.

## 2. Experimental

### 2.1. Materials

Poly($\varepsilon$-caprolactone) of molecular weight 14,000 g/mol ($PCL_L$) was purchased from Sigma–Aldrich (USA). A highly hydrophobic PCL diol ($PCL_H$, $M_{nGPC}$ = 40,400 g/mol; $M_{wGPC}$ = 64,200 g/mol) was synthesized by the microwave-assisted ring-opening polymerization of $\varepsilon$-CL (CL, Sigma–Aldrich) initiated by poly(ethylene glycol) (PEG, molecular weight 400 g/mol, Sigma–Aldrich) and catalyzed by tin(II) 2-ethylhexanoate (SnOct, Sigma–Aldrich) [51]. The PEG content in this copolymer was below 1% in weight, thus resulting in a copolymer with the intrinsic properties of pure PCL [51]. Eudragit® RS 100 (RS, powder, a copolymer of ethylmethacrylate, methylmethacrylate and methacrylic acid esterified with quaternary ammonium groups) and Pluronic F68 were kind gifts of Evonik (Argentina) and BASF (USA), respectively. EFV was a donation of LKM Laboratories (Argentina). $KH_2PO_4$, NaOH, Tween® 80 and solvents were of analytical grade and used as received. Acetonitrile (ACN, HPLC grade, Sintorgan, Argentina) was used as mobile phase in liquid chromatography analyses (see below).

### 2.2. Preparation of EFV-loaded submicron particles

EFV-loaded submicron particles were produced by two methods: (i) nanoprecipitation and (ii) simple oil-in-water (o/w) emulsion and solvent diffusion/evaporation. Regardless of the fact that some of the systems described in the present study were submicron in size, those obtained by precipitation were usually in the 1–200 nm size range.

*Nanoprecipitation*. PCL and Eudragit® RS 100 (1:1 and 1:3 weight ratio, 60 mg total weight) were suspended in acetone (10 mL) and gently heated at 37 °C and stirred, until complete dissolution. Then, EFV (6 mg) was added and thoroughly mixed for 15 min. This solution was poured into a syringe (10 mL) and injected with a needle (21G1, 0.80 mm × 25 mm) on distilled water (20 mL) containing Pluronic F68 (60 mg) at a constant flow rate (20 mL/h, infusion pump PC11U, APEMA, Argentina) under moderate magnetic stirring and at room temperature. The aqueous phase played the role of antisolvent and favored the precipitation of the polymeric particles. The resulting suspension was stirred for 3 h to allow the complete evaporation of the organic solvent and filtered under vacuum through filter paper. Then, samples were frozen at −20 °C and lyophilized (Freeze Dryer Unit GAMMA A, CHRIST®, Germany) for 48 h. The EFV payload was determined by high performance liquid chromatography (HPLC) (see below). Products were stored at room temperature protected from light and moisture until use. Pure PCL and Eudragit® RS 100 particles were also produced as described above. Blank particles (without the incorporation of drug) were used as controls. The different production conditions used are summarized in Table 1.

*Simple oil-in-water (o/w) emulsion and solvent diffusion/evaporation*. Aiming to assess the effect of the solvent on the size and size distribution, two solvents were used. In brief, PCL:Eudragit® RS 100 blends (1:1 weight ratio, 60 mg total weight) were dissolved in dichloromethane (DCM, 5 mL) or ethyl acetate

**Table 1**
Preparation conditions of the different EFV-loaded particles.

| Formulation name | PCL content (mg) | Eudragit content (mg) | Preparation method | Surfactant content (mg) | Homogenization speed (RPM) | Organic phase | |
|---|---|---|---|---|---|---|---|
| | | | | | | Solvent | Volume (mL) |
| $PCL_L$ | 60 | – | | | | | |
| $PCL_L$-RS (1:1) | 30 | 30 | | | | | |
| $PCL_H$-RS (1:1) | 30 | 30 | Nanoprecipitation[a] | 60 | – | Acetone | 10 |
| $PCL_L$-RS (1:3) | 15 | 45 | | | | | |
| RS | – | 60 | | | | | |
| $PCL_L$-RS-EA (1:1) | 30 | 30 | | 60 | 24,000 | Ethyl acetate | |
| | | | | 30 | 24,000 | | |
| | | | oil-in-water (o/w) | 60 | 7200 | | |
| $PCL_L$-RS-DCM (1:1) | 30 | 30 | emulsion | | 20,000 | Dichloromethane | 5 |
| | | | | | 24,000 | | |
| | | | | 90 | 24,000 | | |

$PCL_L$: low molecular weight; $PCL_H$: high molecular weight.
[a] The volume of aqueous phase was, in every case, 20 mL.

(EA, 5 mL). EFV (6 mg) was added to the organic phase and vortexed until complete dissolution. This solution was poured slowly into distilled water (20 mL) containing Pluronic F68 (60 mg) and emulsified by homogenization with a T18 Basic Ultra-Turrax (IKA®-Werke GmbH & Co. KG, Germany) at 24,000 RPM for 5 min. The resulting emulsion o/w was poured into a beaker and stirred until total evaporation of the organic solvent, at room temperature. Then, the sample was vacuum-filtered through filter paper and the suspension was frozen at −20 °C and lyophilized for 48 h (see above). The EFV payload was determined by HPLC (see below). EFV-free particles were prepared and used as controls. To assess the effect of the surfactant concentration and the homogenization speed on the particle size and size distribution, $PCL_L$-RS-DCM (1:1) particles (Table 1) were produced employing three Pluronic F68 concentrations (30, 60 and 90 mg) and homogenization speeds (7200; 20,000 and 24,000 RPM). The different production conditions are presented in Table 1.

### 2.3. Determination of the EFV payload and the entrapment efficiency

The EFV payload in every sample was determined by HPLC (see below). The percentage of EFV payload in the particles, *%EFV*, was calculated from Eq. (1)

$$\%EFV = \frac{W_{EFV}}{W_P} \times 100 \quad (1)$$

where $W_{EFV}$ is the weight of EFV in the particles and $W_P$ is the total weight of particles.

The entrapment efficiency, *%EE*, was calculated according to Eq. (2)

$$\%EE = \frac{EFV_P}{EFV_0} \times 100 \quad (2)$$

where $EFV_P$ is the content of EFV in the particles and $EFV_0$ is the total EFV amount employed in their preparation.

The yield (%) was determined from Eq. (3)

$$\text{Yield} \quad (\%) = \frac{W_P}{W_{pol}} \times 100 \quad (3)$$

where $W_P$ is the total weight of particles obtained after lyophilization and $W_{pol}$ is the total initial amount of polymers employed in their preparation.

Results are reported as mean ± S.D. of three independent experiments.

### 2.4. Characterization of the particles

Size and size distribution (expressed as polydispersity index, PDI) of EFV-free and EFV-loaded particles were determined by Dynamic Light Scattering (DLS, Zetasizer Nano-Zs, Malvern Instruments, UK) provided with a He–Ne (633 nm) laser and a digital correlator ZEN3600. Measurements were conducted at a scattering angle of $\theta = 173°$ to the incident beam and at 25 °C. The surface charge of the different particles was estimated by the zeta-potential (*Z*-pot). Results of intensity mean hydrodynamic diameter ($D_h$), PDI and *Z*-pot are expressed as mean ± S.D. of three independent samples prepared under identical conditions. Data for each single specimen was the result of at least four runs.

The external morphology of lyophilized EFV-free and EFV-loaded particles was visualized by Scanning Electron Microscopy (SEM, FEG-SEM, Zeiss Supra 40 TM apparatus Gemini column, Germany) operating at an accelerating voltage of 3.0 kV. Samples were coated with gold using a sputter coating method. The thickness of the gold layer was between 5 and 10 nm.

### 2.5. Attenuated total reflectance/Fourier transform-infrared spectroscopy (ATR/FT-IR)

The following samples were analyzed by ATR/FT-IR (Nicolet 380 ATR/FT-IR spectrometer, Avatar Combination Kit), Smart Multi-Bounce HATR with ZnSe crystal 45° reflectance (Thermo Scientific, USA) in the range between 4000 and 600 $cm^{-1}$ (15 scans, spectral resolution of 4.0 $cm^{-1}$): (i) pure PCL, pure Eudragit® RS 100, and free EFV, (ii) EFV-free $PCL_L$, $PCL_L$-RS (1:1) and RS particles and (iii) EFV-loaded $PCL_L$, $PCL_L$-RS (1:1) and RS particles. FT-IR spectra were obtained using the OMNIC 8 spectrum software (Thermo Scientific, USA).

### 2.6. Thermal analysis

The thermal analysis was performed by Differential Scanning Calorimetry (DSC, Mettler Toledo TA-400 differential scanning calorimeter, USA). Samples (~5 mg) were sealed in 40 μL Al crucible-pans (Mettler ME-27331, Switzerland) and heated in a simple heating temperature ramp between 25 and 210 °C (10 °C/min) under dry nitrogen atmosphere. The different thermal transitions were analyzed.

### 2.7. In vitro EFV release

The *in vitro* release of EFV from the different particles was assessed by the dialysis bag method over 168 h. Particles containing

3.5–4.5 mg of EFV were dispersed in phosphate-buffered saline (PBS, pH 7.4, 12.5 mL). The resulting suspension was placed into a dialysis bag (regenerated cellulose tubing, molecular weight cut off = 12,000–14,000 g/mol) and placed in a beaker containing the release medium (PBS, pH 7.4 containing 0.5% (w/v) of Tween® 80, 100 mL). Tween® 80 was added to increase the intrinsic solubility of EFV in the release medium and to ensure sink conditions [52]; EFV is poorly water soluble and its intrinsic water solubility is 4 μg/mL [53–55]. Systems were maintained at 37 °C ± 1 under moderate magnetic stirring (200 RPM). At predetermined time intervals, an aliquot of the release medium (20 mL) was withdrawn for EFV analysis and it was replaced by fresh medium pre-heated at 37 °C. The released EFV amounts were quantified by HPLC (see below) and corrected by the volume of release medium withdrawn. Assays were carried out in triplicate and the results are expressed as mean ± S.D. The analysis of the release kinetics and the fitting to different release models was conducted with SigmaPlot® software (SigmaPlot® 2001) and Microsoft® Excel 2003.

The Korsmeyer–Peppas model is a semiempirical model generally used to analyze release data of different pharmaceutical dosage forms and it is expressed by Eq. (4) [56,57]

$$\frac{M_t}{M_\infty} = a \cdot t^n \quad (4)$$

where $M_t$ and $M_\infty$ are the absolute cumulative amount of drug released at time $t$ and at infinite time, respectively, $t$ is the release time, $a$ is the constant incorporating structural and geometric characteristics of the release device and $n$ is the release exponent, indicative of the mechanism of drug release. To determine $n$, only the curve release fraction of $M_t/M_\infty \leq 0.6$ was used. Based on morphological data, particles were considered as spheres [58].

### 2.8. Chromatographic method for EFV

EFV was quantified by HPLC (Alliance HPLC, separation module e2695, Waters, USA) with isocratic flow using a Waters 5 μm, C18, 150 mm × 4.6 mm column (Waters) with a dual-wavelength UV detector (λ = 248 and 252 nm, 2998 Photoiodide Array UV/Vis 2D detector, W2998, Waters, USA); the technique was a modification of a previously reported one [53–55]. The mobile phase of ACN:water (70:30) was pumped at a flow rate of 1.0 mL/min. To determine the EFV payload (%EFV) and the entrapment efficiency (%EE), lyophilized drug-loaded particles (10 mg) were dissolved in ACN (10 mL), conveniently diluted in HPLC mobile phase (1:10) and injected (20 μL) in the HPLC system (see below). For the analysis of the release amounts *in vitro*, aliquots (20 μL) of the release medium withdrawn (20 mL) were injected directly into the HPLC system. EFV concentrations were obtained from a calibration curve with a linearity range between 0.2 and 75 μg/mL (correlation factor was 0.9998–1.0000). Measurements were performed in triplicate and results are expressed as mean ± S.D.

### 2.9. Data analysis

Statistical analysis was performed using one-way ANOVA (5% significance level) combined with Tukey's Multiple Comparison Test (5% significance level). Both analyses were performed using GraphPad Prism version 5.00 for Windows (GraphPad Software, Inc., USA).

## 3. Results and discussion

### 3.1. Preparation and characterization of particles

To target a drug to the CNS by the i.n. route, particles need to fulfill both size and drug payloads requirements [35]. In addition, to ensure constant drug levels over prolonged times, the development of a sustained release system was called for. PCL is a highly biocompatible and biodegradable polyester extensively used to produce different kinds of biomedical devices, including drug delivery systems with a variety of morphologies and tissue engineering scaffolds [36–39]. However, PCL displays relatively high permeability to lipophilic drugs and often relatively sharp burst effects. Eudragit® RS 100 is a water insoluble and permeable cationic poly(methacrylate) copolymer that has been developed to control the release of encapsulated drugs. Even though, these biomaterials are usually employed for the production of oral and topical formulations, previous studies have reported on its good biocompatibility in different parenteral applications [46–49]. Available technologies enable the adjustment of the PCL degradation rate and the drug release rate to fit specific performances by developing copolymers or physical blends, the latter being a more versatile, economic and scalable approach [40].

Aiming to fine tune the particle size and the release kinetics, while maintaining the encapsulation efficiency high, the present work assessed the development of PCL/poly(methacrylate) blend particles and it compared their performance to that of particles made of the pristine counterparts.

Two different methods that have been widely used to prepare polymeric particles containing high cargos of hydrophobic drugs [59], namely nanoprecipitation and simple oil-in-water (o/w) emulsion and solvent diffusion/evaporation, were explored in the present work to encapsulate EFV (Table 1). Nanoprecipitation, also known as the solvent displacement method, is a simple, fast, reproducible, economic and scalable method characterized by the small size and narrow size distribution of the produced particles. On the other hand, solvent diffusion/evaporation was the first method developed to prepare polymeric particles and it is the most widely employed technique to obtain these particles [59].

In the case of nanoprecipitation, acetone was the selected solvent because it effectively solubilized great amounts of both polymers and EFV, while it was miscible with the aqueous phase that served as the antisolvent. Moreover, it was effectively removed by evaporation under normal pressure over a short time [59,60]. In the case of emulsion/solvent diffusion/evaporation method, we evaluated two solvents that display substantially different aqueous solubility; the water solubility of DCM and EA being 2.0% (w/v) and 8.7% (w/v), respectively [61,62].

Regardless of the preparation method and the polymeric composition, the encapsulation efficiency was extremely high, %EE values being greater than 94.5% (Table 2). These values represented %EFV values of approximately 10% (w/w). Differences were not statistically significant ($p < 0.05$) for all the formulations prepared by nanoprecipitation. For example, EFV payloads were 9.5%, 9.8%, 9.4%, 9.8% and 9.9% (w/w) for $PCL_L$, $PCL_H$-RS (1:1), $PCL_L$-RS (1:1), $PCL_L$-RS (1:3) and RS, respectively. Systems produced by the emulsion method showed a similar trend. Furthermore, yields were relatively high and always above 72.5% (Table 2); none of the preparation methods appeared as more efficient than the other.

The different particles were characterized in terms of size, size distribution, *Z*-pot and morphology. Results confirmed that, by adjusting the preparation conditions and the composition, particles of different size and size distribution could be obtained. This parameter was crucial because the size governs the nose-to-brain transport [30,33]. In general, nanoprecipitation led to particles of smaller size than those obtained by emulsion; *e.g.*, the size ranged between 89.5 and 173.9 nm with very small PDI values (0.077–0.276) that were consistent with a unimodal distribution (Table 2 and Fig. 1A). The effect of the PCL molecular weight on the particle size was also evaluated. The greater the molecular weight, the smaller the size of the particles. For example, $PCL_H$-RS (1:1) particles were remarkably smaller ($D_h$ = 93.6 nm)

**Table 2**
Properties of the different EFV-free and EFV-loaded particles.

| Particles | Formulation | Particle size (nm) (±S.D.) | | | | PDI (±S.D.) | *Z*-pot (mV) (±S.D.) | %EFV (±S.D.) | %EE (±S.D.) | Yield (%) (±S.D.) |
|---|---|---|---|---|---|---|---|---|---|---|
| | | Peak 1 | % | Peak 2 | % | | | | | |
| EFV-loaded particles | $PCL_L$ | 173.9 (7.5) | 100 | – | – | 0.077 (0.023) | −17.9 (1.4) | 9.5 (1.3) | 94.8 (13.0) | 75.3 (0.0) |
| | $PCL_H$-RS (1:1) | 93.6 (2.8) | 100 | – | – | 0.115 (0.008) | +32.2 (2.8) | 9.8 (0.8) | 98.4 (7.7) | 87.7 (0.0) |
| | $PCL_L$-RS (1:1) | 144.1 (2.9) | 100 | – | – | 0.126 (0.012) | +35.0 (5.5) | 9.4 (1.6) | 94.5 (15.6) | 90.0 (0.0) |
| | $PCL_L$-RS (1:3) | 117.5 (3.9) | 100 | – | – | 0.151 (0.005) | +37.0 (2.5) | 9.8 (1.7) | 97.6 (17.4) | 72.5 (0.0) |
| | RS | 89.5 (5.3) | 100 | – | – | 0.276 (0.047) | +51.3 (3.9) | 9.9 (1.9) | 99.8 (19.7) | 73.6 (0.0) |
| | $PCL_L$-RS-EA (1:1) | 219.5 (4.9) | 100 | – | – | 0.130 (0.013) | +53.9 (5.6) | 10.9 (0.9) | 108.6 (8.9) | 80.4 (0.0) |
| | $PCL_L$-RS-DCM (1:1) | 83.4 (9.0) | 7.4 | 530.0 (31.8) | 92.6 | 0.352 (0.031) | +53.8 (2.1) | 9.9 (1.3) | 99.9 (13.3) | 72.8 (0.0) |
| EFV-free particles | $PCL_L$ | 171.2 (4.6) | 100 | – | – | 0.052 (0.016) | −15.1 (3.3) | | | |
| | $PCL_H$-RS (1:1) | 90.5 (1.6) | 100 | – | – | 0.123 (0.012) | +30.6 (1.5) | | | |
| | $PCL_L$-RS (1:1) | 145.8 (1.7) | 100 | – | – | 0.137 (0.007) | +33.1 (3.6) | | | |
| | $PCL_L$-RS (1:3) | 110.4 (1.2) | 100 | – | – | 0.139 (0.012) | +32.3 (3.25) | | | |
| | RS | 91.4 (1.3) | 100 | – | – | 0.216 (0.006) | +50.2 (1.0) | | | |
| | $PCL_L$-RS-EA (1:1) | 215.8 (4.0) | 100 | – | – | 0.126 (0.011) | +53.2 (3.3) | | | |
| | $PCL_L$-RS-DCM (1:1) | 71.8 (8.7) | 8.2 | 502.0 (26.9) | 91.8 | 0.299 (0.050) | +53.4 (3.5) | | | |

than $PCL_L$-RS (1:1) ($D_h$ = 144.1 nm) ones. This phenomenon probably relied on the faster precipitation of the high molecular weight PCL of $PCL_H$ owing to its more limited solubility in the acetone/water medium [63]. Interestingly, the addition of increasing amounts of poly(methacrylate) to the formulation resulted in a gradual decrease of the size from 173.9 nm for pure $PCL_L$ particles to 144.1 and 117.5 nm for $PCL_L$-RS (1:1) and $PCL_L$-RS (1:3), respectively. Following the same trend, RS particles were the smallest of all the series with a size of 89.5 nm. These findings were in agreement with previous reports and they would rely on the fact that Eudragit® RS 100 plays the role of surfactant, stabilizing the system and favoring the generation of particles of smaller size [64]. When particles containing identical PCL/poly(methacrylate) ratio (1:1) were produced by the emulsion method, sizes were larger than those obtained by nanoprecipitation. For example, $PCL_L$-RS-EA (1:1) showed a unimodal profile ($D_h$ = 219.5 nm, PDI value = 0.130), while $PCL_L$-RS-DCM (1:1) a bimodal one ($D_{h1}$ = 83.4 nm, 7.4%; $D_{h2}$ = 530.0 nm, 92.6%, PDI = 0.352) (Table 2 and Fig. 1B). In this case, the size of the droplets and consequently of the particle was probably governed by (i) the interfacial tension between the organic and the aqueous phase, (ii) the viscosity of the organic phase and (iii) the diffusion rate of the organic solvent into the aqueous phase [61,64]. Regardless of the fact that the viscosity of DCM and EA are very similar, $PCL_L$-RS-EA (1:1) particles were substantially smaller than those of $PCL_L$-RS-DCM (1:1). EA is more soluble in water and the lower interfacial tension between both phases probably led to smaller droplets than with DCM. This phenomenon together with a faster diffusion into the aqueous phase, prevented droplet coalescence and resulted in a mechanism that combined solvent evaporation/diffusion and precipitation [61,62]. In contrast, DCM is significantly less soluble in water, resulting in higher interfacial tension that favored droplet coalescence and particle size growth [61]. It is worth stressing that the incorporation of EFV did not change the size and size distribution of the particles with respect to EFV-free controls (Table 2).

$PCL_L$-RS-DCM (1:1) particles showed the least optimal properties, namely the largest size and a bimodal size pattern. To assess the ability to reduce the size and the PDI of the particles produced with this solvent, they were produced under three different homogenization speeds: 7200, 20,000 and 24,000 RPM. As expected, the higher the speed, the smaller the size of the particles and the PDI (Table 3). For example, the size decreased from 179.4 nm (27.9%) and 1706.0 (72.1%) at 7200 RPM to 78.5 nm (7.3%) and 531.1 nm (92.7%) at 20,000 RPM; PDI values followed a similar trend with a sharp decrease from 0.739 to 0.495, respectively. A further speed increase to 24,000 RPM did not reduce the size of the particles, values being 83.4 nm (7.4%) and 530.0 nm (92.6%) for both populations. However, the PDI underwent a slight additional decrease to 0.352. Nevertheless, systems always showed two size populations, independently of the speed. Similar results were obtained by Javadzadeh et al. [65]. In this context, we used the highest possible homogenization speed (24,000 RPM) to obtain the smallest particles and the narrowest size distribution of all the systems prepared by this method. The influence of the surfactant concentration on the size and size distribution of $PCL_L$-RS-DCM (1:1) particles was also assessed. The increase of Pluronic® F68 concentration from 30 to 60 mg per batch resulted in a decrease of the size from 93.4 nm (10.0%) and 597.7 nm (90.0%) to 83.4 nm

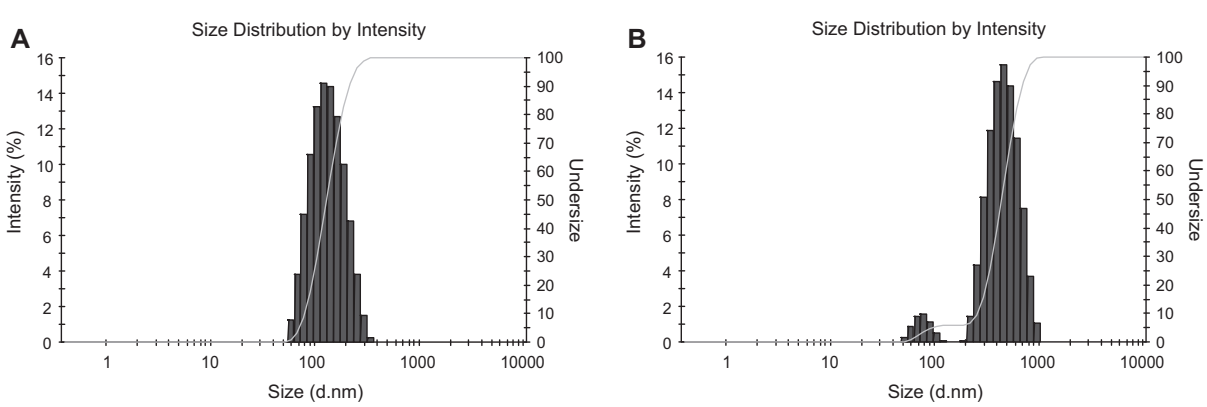


**Fig. 1.** Particle size distribution of EFV-loaded particles. (A) $PCL_L$-RS (1:1) produced by nanoprecipitation and (B) $PCL_L$-RS-DCM (1:1) produced by simple o/w emulsion and solvent diffusion/evaporation method.

**Table 3**
Effect of homogenization speed and surfactant (Pluronic® F68) concentration on the size of $PCL_L$-RS-DCM (1:1) particles.

| Homogenization speed (RPM) | Particle size | | | | | | Surfactant (mg)[b] | Particle size | | | | | |
|---|---|---|---|---|---|---|---|---|---|---|---|---|---|
| | Peak 1[a] | | Peak 2 | | PDI (±S.D.) | Z-pot (mV) (±S.D.) | | Peak 1 | | Peak 2 | | PDI (±S.D.) | Z-pot (mV) (±S.D.) |
| | $D_h$ (nm) (±S.D.) | % | $D_h$ (nm) (±S.D.) | % | | | | $D_h$ (nm) (±S.D.) | % | $D_h$ (nm) (±S.D.) | % | | |
| 7200 | 179.4 (17.6) | 27.9 | 1706.0 (196.7) | 72.1 | 0.739 (0.159) | +54.3 (1.6) | 30 | 93.4 (21.7) | 10.0 | 597.7 (56.1) | 90.0 | 0.402 (0.101) | +56.2 (0.8) |
| 20,000 | 78.5 (10.0) | 7.3 | 531.1 (21.7) | 92.7 | 0.495 (0.022) | +55.1 (1.4) | 60 | 83.4 (9.0) | 7.4 | 530.0 (31.8) | 92.6 | 0.352 (0.031) | +53.8 (2.1) |
| 24,000 | 83.4 (9.0) | 7.4 | 530.0 (31.8) | 92.6 | 0.352 (0.031) | +53.8 (2.1) | 90 | 88.0 (4.7) | 7.0 | 506.4 (43.6) | 93.0 | 0.306 (0.057) | +59.7 (1.6) |

[a] The surfactant content per batch in assays with different homogenization speeds was 60 mg.
[b] The homogenization speed in assays with different surfactant concentrations was 24,000 RPM.

(7.4%) and 530.0 nm (92.6%), respectively. A further increase in the amount to 90 mg/batch did not change the size substantially. Interestingly, particles prepared by nanoprecipitation and $PCL_L$-RS-EA (1:1) presented a size range that could fit the demands for intranasal administration and efficient transport to the CNS [30,31]. Conversely, the size of $PCL_L$-RS-DCM (1:1) particles would be slightly larger than the upper limit of 300 nm.

*Z*-pot is a measure of the charge density on the surface and it is intimately associated with the concentration of charged moieties and the size of the particle [66]. $PCL_L$ showed a negative value of −17.9 mV probably due to the superficial availability of —COOH groups (Table 2). Conversely, all the blend formulations were positively charged; values were between +32.2 and +37.0 mV and +53.8 and +53.9 mV for particles produced by nanoprecipitation and emulsion, respectively. This behavior relied on the incorporation of the polycationic Eudragit® RS 100 that displays pendant quaternary ammonium moieties [45]; pure RS particles showed a positive surface charge (+51.3 mV). It is worth stressing that *Z*-pot values of $PCL_L$-RS-EA (1:1), $PCL_L$-RS-DCM (1:1) were identical and very similar to that of RS particles. These data strongly suggested that in the emulsion method, Eudragit® RS 100 accommodated at the organic solvent/water interface, playing the role of surfactant and conferring a more positively charged surface than in nanoprecipitation [64]. Interestingly, the incorporation of 50% (w/w) poly(methacrylate) into the formulation was sufficient to switch the *Z*-pot value from mildly negative ($PCL_L$) to strongly positive.

The presence of positively charged surface led to two main outcomes. On the one hand, it physically stabilized the colloidal systems over time; the size and size distribution of the particles remained unaltered over 1 month (data not shown). A positive *Z*-pot value would also play a key role in the interaction with mucin glycoprotein of the mucus of nasal cavity that is a negatively charged molecule [50,67], thus resulting in more prolonged contact time and more efficient nasal absorption. Moreover, the well-established mucoadhesive characteristics of Eudragit® RS 100 will further contribute to extend the residence time in the nose [50]. Finally, the interaction of positively charged particles with negatively charged epithelia would help to open tight junctions and facilitate the absorption of drugs by the paracellular pathway [68].

To characterize the morphology, representative particles were visualized by SEM. Fig. 2 exemplifies the results for EFV-loaded $PCL_L$, $PCL_H$-RS (1:1) and PCL-RS-DCM (1:1) and EFV-free PCL-RS-DCM (1:1) particles. Irrespectively of the composition and the production method, particles were spherical and sizes were in good agreement with DLS data. Furthermore, EFV crystals could not be visualized neither outside the particles nor on the surface, indicating that the drug was completely encapsulated. It is worth stressing that the incorporation of EFV did not change the size pattern and the *Z*-pot of the particles (Fig. 2C and D).

Overall %EFV, %EE and size and size distribution results indicated that nanoprecipitation was a very efficient encapsulation technique that owing to its simplicity, reproducibility and potential scalability emerged as more appealing than the emulsion one.

### 3.2. ATR/FT-IR analysis

To characterize the interaction between the polymer matrix and the encapsulated drug, samples of the different EFV-free and EFV-loaded particles produced by nanoprecipitation were studied by ATR/FT-IR spectroscopy and compared to the spectrum of the pristine components, namely free EFV, pure PCL and pure poly(methacrylate). This study was of interest due to the potential hydrophobic interactions between C—F groups of EFV with carbonyl groups in the backbone of PCL and the poly(methacrylate) that could influence the release kinetics.

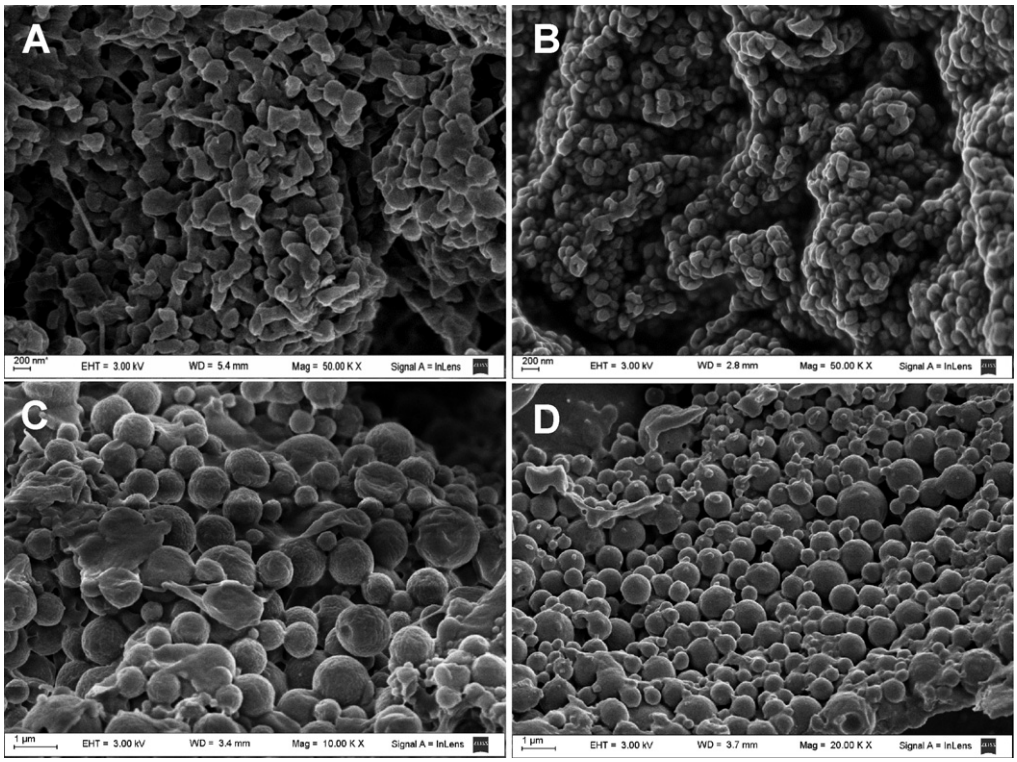


**Fig. 2.** SEM micrographs of EFV-loaded (A–C) and EFV-free particles (D). (A) $PCL_L$, (B) $PCL_H$-RS (1:1), (C) $PCL_L$-RS-DCM (1:1) and (D) EFV-free $PCL_L$-RS-DCM (1:1). Scale bar: (A) and (B) = 200 nm; (B) and (C) = 1 μm.

Free EFV showed the characteristic bands of (i) —NH stretching of the benzoxazin-2-one ring at 3311 $cm^{-1}$, (ii) C—C triple bond stretching at 2250 $cm^{-1}$, (iii) C=O stretching at 1749 $cm^{-1}$, C=C stretching at 1602 $cm^{-1}$ (iv) C—F stretching at 1186–1197 $cm^{-1}$. Pure PCL and $PCL_L$ particles showed bands of the carbonyl groups at 1725 $cm^{-1}$ that were characteristic of crystalline PCL [69,70], indicating that the production process did not altered the crystallinity of the polyester. Pure Eudragit and RS particles displayed the typical signal of C=O at 1724 and 1729 $cm^{-1}$, respectively. An EFV:PCL physical mixture (1:9) showed the characteristic bands of both the drug and the polymer, indicating that the drug was detectable by this technique. Then, spectra of EFV-loaded $PCL_L$, $PCL_L$-RS (1:1) and RS particles showed only the characteristic bands of the polymers; *e.g.*, the C=O stretching was observed without any shifting at 1725–1727 $cm^{-1}$. An EFV-free $PCL_L$-RS (1:1) system showed the same spectrum. These findings suggested that the possible C—F/C=O interactions were negligible. Moreover, the bands of EFV in the particles were not apparent, indicating the effective encapsulation of the drug within the polymeric matrix. These findings were in full agreement with SEM analysis.

### 3.3. Thermal analysis

DSC is a gold standard technique to study the nature of drugs encapsulated within a polymeric matrix and to elucidate whether they are in a crystalline or amorphous state. All the blend particles showed a characteristic bimodal transition of PCL with two melting endotherms at 47–48 °C and 54–55 °C that indicated the presence of two crystalline fractions, the thermal behavior being identical to that of $PCL_L$ (Table 4). These results were in agreement with the literature [69]. The $T_g$ of Eudragit® RS 100 at 58 °C was identified only in RS samples probably because this peak overlapped with the $T_m$ of PCL. The $T_m$ of EFV at 135 °C was not apparent, suggesting that the drug underwent amorphization during the encapsulation process. However, the analysis of a representative physical mixture that contained the same composition of the particles showed that, despite the high drug payload, EFV was not detectable by DSC in these systems.

### 3.4. In vitro EFV release

The goal of encapsulating EFV within polymeric particles was to sustain the release over a longer time when compared to polymeric micelles [53,54]. To comparatively assess the EFV release kinetics in the different systems, an amount of EFV-loaded particles containing a constant EFV payload (3.5–4.5 mg) was dispersed in the release medium and dialyzed against PBS (pH 7.4, 37 °C). The released EFV amounts were monitored over 168 h (Fig. 3). This dilution ensured the maintenance of the sink conditions [53–55].

$PCL_L$ particles presented the faster release rate of all the systems with a greater burst effect. The addition of increasing Eudragit® RS 100 concentrations led to a substantial decrease of the burst effect and to a more sustained release over time. For example, $PCL_L$ released 32.6% at 24 h, while $PCL_L$-RS (1:1), $PCL_L$-RS (1:3) and RS released 22.3%, 19.7%, and 15.3%, respectively, in the same time interval (Fig. 3A); these percentages represented the release of 1050, 750, 690 and 540 μg of EFV, respectively, at 24 h (Fig. 4). These findings were in agreement with the results obtained by Hoffart et al. [71]. Eudragit® RS 100 is insoluble in water and it does not undergo swelling. However, the presence of quaternary ammonium groups increases its water permeability, making it appropriate for the development of sustained release formulations. Particles prepared with high molecular weight PCL ($PCL_H$-RS (1:1)) released approximately 17% of the payload (600 μg) at 24 h (Fig. 3A), this level being moderately lower than that of a similar system made of low molecular weight PCL, $PCL_L$-RS (1:1). At later time points, both samples showed a very similar release pattern, independently of the particle size. Thus, the difference at the initial stages of the release would mainly stem from the presence of a more compact and less permeable polymer matrix in $PCL_H$-RS (1:1). In

**Table 4**
Thermal analysis of the different EFV-loaded particles.

| Sample | Physical mixture[a] | $PCL_L$ | | $PCL_L$-RS (1:1) | | $PCL_H$-RS (1:1) | | $PCL_L$-RS-EA (1:1) | |
|---|---|---|---|---|---|---|---|---|---|
| | | Peak 1 | Peak 2 | Peak 1 | Peak 2 | Peak 1 | Peak 2 | Peak 1 | Peak 2 |
| $T_m$ (°C) | 60.1 | 47.2 | 53.9 | 47.5 | 53.8 | 48.0 | 54.7 | 47.6 | 54.2 |

RS particles showed $T_g$ at 58 °C.
[a] The physical mixture contained an EFV:PCL 1:9 weight ratio.

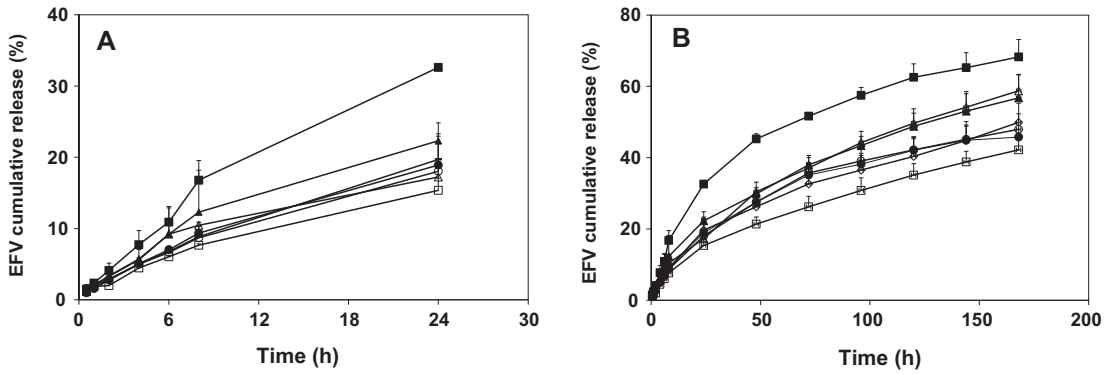


**Fig. 3.** EFV cumulative release from different drug-loaded particles prepared by the nanoprecipitation and the emulsion technique over (A) 24 h and (B) 168 h. $PCL_L$ (■), $PCL_H$-RS (1:1) (△), $PCL_L$-RS (1:1) (▲), $PCL_L$-RS (1:3) (◊), $PCL_L$-RS-EA (1:1) (○), $PCL_L$-RS-DCM (1:1) (●) and RS (□). Data are reported as mean ± S.D. ($n$ = 3).

the case of particles produced by the emulsion method, both release profiles were almost superimposable. Also here, the remarkable difference in particle size between $PCL_L$-RS-EA (1:1) and $PCL_L$-RS-DCM (1:1) (Table 2) did not affect the release performance substantially (Fig. 3). In addition, these results were similar to those of $PCL_L$-RS (1:1) prepared by nanoprecipitation (Fig. 3), strongly suggesting that the release profile was mainly influenced by the composition of the polymer blend and not by the preparation technique. Interestingly, the particle composition emerged as the most relevant parameter governing the release profile, especially during the first 24 h, where the incorporation of Eudragit® RS 100 diminished the released amounts (Fig. 4). Later on, the release was similar for all the particles, regardless of their composition. Remarkably, the release was prolonged for more than one week, making these systems optimal for the sustained release of the encapsulated drug in the CNS.

The drug release from polymeric carriers is a complex process that combines drug diffusion, polymer chain relaxation and erosion phenomena [72]. To further understand the phenomena involved in the release process, data were analyzed by different release models (Table 5). In all cases, the release kinetics fitted the Higuchi model with $R^2_{adj}$ values >0.9779 (Table 5). These findings suggested that the release was mainly controlled by diffusion. To gain further insight into the mechanisms governing the release, data were also analyzed by the Korsmeyer–Peppas model, particles being considered as spheres [58]. In this model, $n$ values of 0.43 indicate that the drug release is controlled by Fickian diffusion. Conversely, $n$ values between 0.43 and 0.85 reveal a non-Fickian diffusion process, known as anomalous transport [73]; the release can be attributed to a combination of drug diffusion and polymer chain relaxation as the solvent diffuse into the polymeric matrix. Finally, $n \geq 0.85$ indicates a supercase II transport where the drug release is purely governed by polymer relaxation [40]. All the particles under study showed $n$ values in the 0.520–0.587 range. These results indicated that the drug release was accomplished by the combination of two phenomena: diffusion of the drug and polymer chain relaxation. Even though hydrophobic interactions between the $CF_3$ group of EFV and carbonyl groups in the backbone of PCL and poly(methacrylate) could play a role in the release process, ATR/FT-IR data strongly suggested the absence of these interactions.

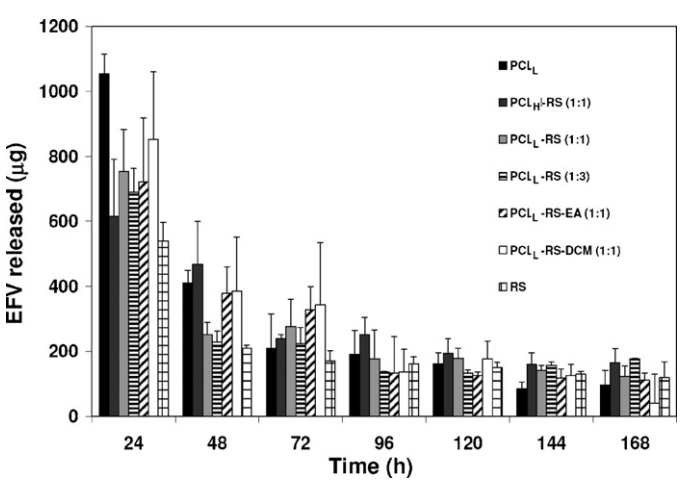


**Fig. 4.** Comparative daily EFV release from the different EFV-loaded particles over 168 h. Data are reported as mean ± S.D. ($n$ = 3).

**Table 5**
Curve fitting analysis of EFV-loaded particles.

| Formulation | Higuchi model | | Korsmeyer–Peppas model | | |
|---|---|---|---|---|---|
| | $D$ (cm² h⁻¹) | $R^2_{adj}$ | $k$ | $n$ | $R^2_{adj}$ |
| $PCL_L$ | 5.8127 | 0.9779 | 0.048 | 0.555 | 0.9794 |
| $PCL_L$-RS (1:1) | 4.6223 | 0.9963 | 0.037 | 0.538 | 0.9957 |
| $PCL_H$-RS (1:1) | 4.7876 | 0.9977 | 0.030 | 0.587 | 0.9971 |
| $PCL_L$-RS (1:3) | 3.9707 | 0.9968 | 0.030 | 0.548 | 0.9946 |
| RS | 3.3778 | 0.9989 | 0.023 | 0.568 | 0.9981 |
| $PCL_L$-RS-EA (1:1) | 4.0677 | 0.9925 | 0.032 | 0.540 | 0.9885 |
| $PCL_L$-RS-DCM (1:1) | 3.9560 | 0.9867 | 0.034 | 0.520 | 0.9864 |

Higuchi model: $D$, diffusion rate constant.
Korsmeyer–Peppas model: analysis was conducted for $M_t/M_\infty \leq 0.6$; k, kinetic constant; $n$, release exponent.

## 4. Conclusions

The present explored the encapsulation of the antiretroviral EFV within pure PCL, pure Eudragit® RS 100 and PCL/Eudragit® RS 100 blend particles by two different methods. Regardless of the polymer composition and the production technique, all the systems displayed remarkably high encapsulation efficiency and drug payload. On the other hand, nanoprecipitation resulted in smaller particles and narrower size distribution patterns. These data together with the greater simplicity, reproducibility and eventually scalability in an industrial setup, make this method more advantageous than the traditional emulsion one. The incorporation of the poly(methacrylate) enabled the fine tuning of the particle size and the release kinetics; the greater the poly(methacrylate) content, the less pronounced the burst effect and the more sustained the release. Moreover, the incorporation of poly(methacrylate) changed the *Z*-pot from mildly negative to strongly positive values. This change would be beneficial to improve the residence time of the particles in contact with the nasal mucosa. Interestingly, substantial differences in the size of the particles did not lead to concomitant changes in the release profile, the composition emerging as the main parameter that controlled the burst effect. Since the size and composition have been pointed out as relevant features that govern the nose-to-brain transport, future work will investigate the performance of EFV-loaded particles of different size produced by nanoprecipitation in an animal model.

## Acknowledgments

KPS thanks a Ph.D. scholarship of CONICET. DAC and AS are staff members of CONICET. The work was partially supported by grants of UBA (UBACyT 20020090200189) and CONICET (PIP0220). Authors thank Dr. Romina J. Glisoni for technical assistance in ATR/FT-IR analysis.

## References

[1] AIDS Epidemic Update 2007, World Health Organization. http://www.who.int/hiv/epiupdates/en/index.html (accessed 07.2009).
[2] Panel on Clinical Practices for Treatment of HIV Infection, Pan. Am. J. Public Health 10 (2001) 426.
[3] UNAIDS/WHO AIDS Epidemic. http://www.unaids.org/en/HIV (accessed 07.2009).
[4] M. Delaney, Retrovirology 3 (2006) S6.
[5] L. Andrews, G. Friedland, Infect. Dis. Clin. North Am. 14 (2000) 1.
[6] F. Romanelli, A.D. Hoven, Curr. Pharm. Des. 12 (2006) 1121.
[7] S. Park, P.J. Sinko, J. Pharmacol. Exp. Ther. 312 (2005) 1249.
[8] L. Geeraert, G. Kraus, R.J. Pomerantz, Annu. Rev. Med. 59 (2008) 487.
[9] G. Peralta, M.B. Sánchez, S. Echevarría, E.M. Valdizán, J.A. Armijo, Enferm. Infecc. Microbiol. Clin. 26 (2008) 150.
[10] M. Dean, Y. Hamon, G. Chimini, J. Lipid Res. 42 (2001) 1007.
[11] C.F. Higgins, Nature 446 (2007) 749.
[12] B.J. Aungst, Adv. Drug Deliv. Rev. 39 (1999) 105.
[13] P.V. Balimane, P.J. Sinko, Adv. Drug Deliv. Rev. 39 (1999) 183.
[14] R.N. Peroni, S.S. Di Gennaro, C. Hocht, D.A. Chiappetta, M.C. Rubio, A. Sosnik, G.F. Bramuglia, Biochem. Pharmacol. 82 (2011) 1227.
[15] P.T. Ronaldson, Y. Persidsky, R. Bendayan, Glia 56 (2008) 1711.
[16] P. Vivithanaporn, M.J. Gill, C. Power, Expert Rev. Anti Infect. Ther. 9 (2011) 371.
[17] A. Nath, N. Sacktor, Curr. Opin. Neurol. 19 (2006) 358.
[18] L. Crews, C. Patrick, C.L. Achim, I.P. Everall, E. Masliah, Int. J. Mol. Sci. 10 (2009) 1045.
[19] P.K. Dash, S. Gorantla, H.E. Gendelman, J. Knibbe, G.P. Casale, E. Makarov, A.A. Epstein, H.A. Gelbard, M.D. Boska, L.Y. Poluektova, J. Neurosci. 31 (2011) 3148.
[20] K. Grovit-Ferbas, M.E. Harris-White, Immunol. Res. 48 (2010) 40.
[21] A. Van Rie, A. Mupuala, A. Dow, Pediatrics 122 (2008) 123.
[22] J. Cook-Easterwood, L.D. Middaugh, W.C. Griffin 3rd, I. Khan, W.R. Tyor, Exp. Neurol. 205 (2007) 506.
[23] A. Sosnik, D.A. Chiappetta, A.M. Carcaboso, J. Control. Release 138 (2009) 2.
[24] H.L. Wong, N. Chattopadhyay, X.Y. Wu, R. Bendayan, Adv. Drug Deliv. Rev. 62 (2010) 503.
[25] S. Gunaseelan, K. Gunaseelan, M. Deshmukh, X. Zhang, P.J. Sinko, Adv. Drug Deliv. Rev. 62 (2010) 518.
[26] D.A. Chiappetta, A. Sosnik, Eur. J. Pharm. Biopharm. 66 (2007) 303.
[27] N. Shaik, G. Pan, W.F. Elmquist, J. Pharm. Sci. 97 (2008) 5421.
[28] N. Shaik, N. Giri, W.F. Elmquist, J. Pharm. Sci. 98 (2009) 4170.
[29] A. Nowacek, H.E. Gendelman, Nanomedicine (Lond.) 4 (2009) 557.
[30] A. Mistry, S. Stolnik, L. Illum, Int. J. Pharm. 379 (2009) 146.
[31] S.V. Dhuria, L.R. Hanson, W.H. Frey 2nd, J. Pharm. Sci. 99 (2010) 1654.
[32] L.R. Hanson, W.H. Frey 2nd, J. Neuroimmune Pharmacol. 2 (2007) 81.
[33] L. Illum, J. Pharm. Pharmacol. 56 (2004) 3.
[34] A.M. Al-Ghananeem, H. Saeed, R. Florence, R.A. Yokel, A.H. Malkawi, J. Drug Target. 18 (2010) 381.
[35] D.A. Chiappetta, C. Hocht, J.A.W. Opezzo, A. Sosnik, Nanomedicine-UK, in press.
[36] D. Perrin, J. English, Polycaprolactone, in: A. Domb, Y. Kost, D. Wiseman (Eds.), Handbook of Biodegradable Polymers. Drug Targeting and Delivery, vol. 7, 1997, pp. 63–77.
[37] N. Kumar, M.N.V. Ravikumar, A.J. Domb, Adv. Drug Deliv. Rev. 53 (2001) 23.
[38] M.J. Rathbone, C.R. Bunta, C.R. Oglea, S. Burggraafa, K.L. Macmillanb, K. Pickering, J. Control. Release 85 (2002) 61.
[39] M.A. Wooddruff, D.W. Hutmacher, Prog. Polym. Sci. 35 (2010) 1217.
[40] A.M. Puga, A. Rico-Rey, B. Magariños, C. Alvarez-Lorenz, A. Concheiro, Acta Biomater. 8 (2012) 1507.
[41] H. Sun, L. Mei, C. Song, X. Cui, P. Wang, Biomaterials 27 (2006) 1735.
[42] J.L. Bourges, C. Bloquel, A. Thomas, F. Froussart, A. Bochot, F. Azan, R. Gurny, D. BenEzra, F. Behar-Cohen, Adv. Drug Deliv. Rev. 58 (2006) 1182.
[43] J.S. Chawla, M.M. Amiji, Int. J. Pharm. 249 (2002) 127.
[44] J. Chen, A. Ma, Y. Lai, Y. Chen, M. Cui, J. Biomed. Eng. 14 (1997) 334.
[45] H. Eidi, O. Joubert, G. Attik, R.E. Duval, M.C. Bottin, A. Hamouia, P. Maincent, B.H. Rihn, Int. J. Pharm. 396 (2010) 156.
[46] S.R. Schaffazick, I.R. Siqueira, A.S. Badejo, D.S. Jornada, A.R. Pohlmann, C.A. Netto, S.S. Guterres, Eur. J. Pharm. Biopharm. 69 (2008) 64.
[47] A. Basarkar, J. Singh, Pharm. Res. 26 (2009) 72.
[48] A.C. Zago, J.C. Raudales, G. Attizzani, B.S. Matte, G.I. Yamamoto, J.A. Balvedi, L. Nascimento, B.G. Kosachenco, P.R. Centeno, A.J. Zago, Catheter. Cardiovasc. Interv. (2012), http://dx.doi.org/10.1002/ccd.24331.
[49] A. Rolland, R. Le Verge, B. Collet, L. Toujas, J. Pharm. Sci. 78 (1989) 781.
[50] A. Lopedota, A. Trapani, A. Cutrignelli, L. Chiarantini, E. Pantucci, R. Curci, E. Manuali, G. Trapani, Eur. J. Pharm. Biopharm. 72 (2009) 509.
[51] G. Gotelli, P. Bonelli, G. Abraham, A. Sosnik, J. Appl. Polym. Sci. 121 (2011) 1321.
[52] L.K. Shah, M.M. Amiji, Pharm. Res. 23 (2006) 2638.
[53] D.A. Chiappetta, C. Hocht, C. Taira, A. Sosnik, A Nanomedicine-UK 5 (2010) 11.
[54] D.A. Chiappetta, C. Alvarez-Lorenzo, A. Rey-Rico, P. Taboada, A. Concheiro, A. Sosnik, Eur. J. Pharm. Biopharm. 76 (2010) 24.
[55] D.A. Chiappetta, C. Hocht, C. Taira, A. Sosnik, Biomaterials 32 (2011) 2379.
[56] P.L. Ritger, N.A. Peppas, J. Control. Release 5 (1987) 23.
[57] P.L. Ritger, N.A. Peppas, J.Control. Release 5 (1987) 37.
[58] V. Sanna, A.M. Roggio, A.M. Posadino, A. Cossu, S. Marceddu, A. Mariani, V. Alzari, S. Uzzau, G. Pintus, M. Sechi, Nanoscale Res. Lett. 28 (2011) 260.
[59] J. Prasad Rao, K.E. Geckeler, Prog. Polym. Sci. 36 (2011) 887.
[60] M.A. Moretton, R.J. Glisoni, D.A. Chiappetta, A. Sosnik, Colloids Surf. B: Biointerfaces 79 (2010) 467.
[61] K.C. Song, H.S. Lee, I.Y. Choung, K.I. Cho, Y. Ahn, E.J. Choi, Colloids Surf. A: Physicochem. Eng. Aspects 276 (2006) 162.
[62] J. Zhao, C.S. Liu, Y. Yuan, X.Y. Tao, X.Q. Shan, Y. Sheng, F. Wu, Biomaterials 28 (2007) 1414.
[63] F. Lince, D.L. Marchisio, A.A. Barresi, J. Colloid Interface Sci. 322 (2008) 505.
[64] Y.V. Chernysheva, V.G. Babak, N.R. Kildeeva, F. Boury, J.P. Benoit, N. Ubrich, P. Maincent, Mendeleev Commun. 13 (2003) 65.
[65] Y. Javadzadeh, F. Ahadi, S. Davaran, G. Mohammadi, A. Sabzevari, K. Adibkia, Colloids Surf. B: Biointerfaces 81 (2010) 498.
[66] Y. Chen, G. Cui, M. Zhao, C. Wang, K. Qian, S. Morris-Natschke, K.-H. Lee, S. Peng, Bioorg. Med. Chem. 16 (2008) 5914.
[67] D. Pawar, A.K. Goyal, S. Mangal, N. Mishra, B. Vaidya, S. Tiwari, A.K. Jain, S.P. Vyas, AAPS J. 12 (2010) 130.
[68] J. Wang, Y. Tabata, K. Morimoto, J. Control. Release 113 (2006) 31.
[69] A. Sosnik, D. Cohn, Polymer 44 (2003) 7033.
[70] D. Cohn, G. Lando, A. Sosnik, S. Garty, A. Levi, Biomaterials 27 (2006) 1718.
[71] V. Hoffart, N. Ubrich, C. Simonin, V. Babak, C. Vigneron, M. Hoffman, T. Lecompte, F. Maincent, Drug Dev. Ind. Pharm. 28 (2002) 1091.
[72] B.P. Bastakoti, S. Guragain, Y. Yokoyama, S.I. Yusa, K. Nakashima, Colloids Surf. B: Biointerfaces 88 (2011) 734.
[73] P. Costa, J.M. Sousa Lobo, Eur. J. Pharm. Sci. 13 (2001) 123.